PCCP

Stability of *n*-alkanes and *n*-perfluoroalkanes against horizontal displacement on a graphite surface

Journal:	*Physical Chemistry Chemical Physics*
Manuscript ID	CP-ART-06-2024-002418.R2
Article Type:	Paper
Date Submitted by the Author:	03-Sep-2024
Complete List of Authors:	Kikkawa, Yoshihiro; National Institute of Advanced Industrial Science and Technology (AIST), Tsuzuki, Seiji; The University of Tokyo, Applied Physics; Yokohama National University, Institute of Advanced Sciences

ARTICLE

Stability of *n*-alkanes and *n*-perfluoroalkanes against horizontal displacement on a graphite surface

Received 00th January 20xx,
Accepted 00th January 20xx

DOI: 10.1039/x0xx00000x

Yoshihiro Kikkawa[a]* and Seiji Tsuzuki[b]*

The stability of adsorbed molecules on surfaces is fundamental and important for various applications, such as coating, lubrication, friction, and self-assembled structure formation. In this study, we investigated the structures and interaction energies (E_{int}) of propane, *n*-pentane, *n*-heptane, perfluoropropane, *n*-perfluoropentane, and *n*-perfluoroheptane adsorbed on the surface of $C_{96}H_{24}$ (a model surface of graphite). The changes in E_{int} ($\Delta E_{int} = E_{int} - E_{int}(0)$) associated with the horizontal displacement from the stable position were calculated using dispersion-corrected density functional theory (DFT; B3LYP-D3), where $E_{int}(0)$ is the E_{int} at the stable position. The maximum value of ΔE_{int} ($\Delta E_{int(max)}$) associated with the horizontal displacement increased as the chain length increased. The $\Delta E_{int(max)}$ for the three *n*-alkanes were 1.10, 1.82, and 2.35 kcal mol^{-1}, respectively. The values for *n*-perfluoroalkanes were 0.57, 0.83, and 1.04 kcal mol^{-1}, respectively. The $\Delta E_{int(max)}$ values for the *n*-alkanes were significantly larger than those for the corresponding *n*-perfluoroalkanes. The $E_{int(max)}$ value per carbon atom of the *n*-alkanes (ca. 0.30 kcal mol^{-1}) is approximately 2.5 times as large as that of *n*-perfluoroalkanes (ca. 0.12 kcal mol^{-1}). The ΔE_{int} associated with the horizontal displacement of propane and perfluoropropane on circumcoronene ($C_{54}H_{18}$) obtained by the B3LYP-D3 calculations are close to those obtained by the second order Møller–Plesset (MP2) and dispersion-corrected double hybrid DFT calculations, suggesting the sufficient accuracy of the ΔE_{int} obtained by the B3LYP-D3. Thus, our quantitative analysis revealed the higher stability of *n*-alkanes against horizontal displacement on a graphite surface than that of *n*-perfluoroalkanes.

Introduction

The analysis of the structures and stability of adsorbed molecules on solid surfaces is important from both basic and applied science perspectives, such as coating, lubrication, friction, and self-assembled structure formations.[1–4] For example, lubricants are used to prevent direct contact between material surfaces, resulting in the reduction of friction and wear. The most common constituents of lubricants are alkyl and fluoroalkyl moieties,[5–9] which physisorbed on the surfaces of sliding materials. It is important to understand the interactions between constituent molecules and the substrate, and their stability on surfaces, which relates to the durability of the surface functionality, to fabricate an interface with tailored surface properties.

Alkyl chains are often included as substituents in organic compounds and play an important role in intermolecular interactions, which significantly affect material characteristics, such as reactivity, physical properties, and assembled structures.[10–13] Recently, many carbon-based materials have been developed; therefore, understanding the interactions between graphitic materials and organic compounds containing alkyl chains has become an interesting subject of research.[14–18] In this context, several experimental[19–24] and theoretical studies[25–30] related to the adsorption of alkanes on graphite have been reported thus far.

Particular to the two-dimensional self-assemblies at the highly oriented pyrolytic graphite (HOPG)/solvent interface, scanning tunnelling microscopy (STM) has revealed the molecular arrangements of the building blocks containing alkyl chains.[31-34] The alkyl chains can have flat-on and edge-on orientations, in which the mean planes of all trans zigzag main-chain backbone are parallel (flat-on) and perpendicular (edge-on) to the surface plane of the substrate, respectively. When *n*-alkyl chains adsorb to HOPG, a flat-on orientation is preferred over an edge-on orientation.[30, 35,36]

In STM studies, partially fluorinated alkyl chains have played as chemical markers to distinguish them from normal alkyl chains because the image contrast of fluorinated moiety is darker than that of normal alkyl chains.[37–43] For example, we previously investigated the two-dimensional self-assembly of an isobutenyl ether compound possessing semi-fluoroalkyl chains.[43] Although the blend system enabled the formation of a stable physisorbed monolayer owing to the interdigitation of the semi-fluoroalkyl and normal alkyl chains, the two-dimensional structure of a single component molecule with a

[a] *National Institute of Advanced Industrial Science and Technology (AIST), Tsukuba Central 5, 1-1-1 Higashi, Tsukuba, Ibaraki 305-8565, Japan E-mail: y.kikkawa@aist.go.jp*
[b] *Department of Applied Physics, The university of Tokyo, Tokyo 113-8656, Japan E-mail: tsuzuki.seiji@mail.u-tokyo.ac.jp.*

Electronic Supplementary Information (ESI) available: Comparison of E_{int} and ΔE_{int} values obtained by B3LYP-D3, PBE0-D3, BLYP-D3, dispersion-corrected double hybrid DFT and MP2 calculations, Two-dimensional scan of ΔE_{int}, Optimised geometries of $C_{96}H_{24}$ complexes with *n*-alkanes and *n*-perfluoroalkanes, E_{int} and ΔE_{int} values at each displacement along *x*- and *y*-axes, Cause of ΔE_{int} change by horizontal displacement. See DOI: 10.1039/x0xx00000x

semi-fluoroalkyl moiety could not be observed by STM at the HOPG/1-phenyloctane interface. Less adsorption ability of *n*-fluoroalkanes on the HOPG surface than *n*-alkanes have also been reported by the competitive adsorption experiment in a binary mixture of them.[44] The calculated adsorption energies of *n*-fluoroalkanes on circumcoronene: $C_{54}H_{18}$ (graphite model surface) are smaller than those of the corresponding *n*-alkanes.[30] The stability of self-assembled monolayers of *n*-alkanes and *n*-fluoroalkanes on graphite will be influenced not only by the magnitude of the adsorption energies, but also by the stability of adsorbed molecules against horizontal displacement on the surface.

As stated above, several experimental and theoretical studies have been performed for molecules adsorbed at optimal and stable positions on graphitic surfaces. However, to our knowledge, no measurements have been reported on the barrier heights associated with the horizontal motion of molecules on graphite, which are important for immobilizing the adsorbed molecules and thus for self-assembly formation at the surface. In this study, we evaluated the change in the interaction energies (ΔE_{int}) of *n*-alkanes and *n*-perfluoroalkanes on the surface of $C_{54}H_{18}$ and $C_{96}H_{24}$, which are models of the graphite surface, associated with horizontal displacement by dispersion-corrected density functional theory (DFT) and second order Møller–Plesset (MP2) calculations. The effects of chain length and fluorination on the changes in calculated E_{int} were analysed. Based on the results, we discussed the stability of adsorbed *n*-alkanes and *n*-perfluoroalkanes on a graphitic material against horizontal displacement.

Computational details

Gaussian 16 software (Gaussian, Wallingford, CT, USA) was used for DFT and MP2 calculations.[45] The geometries of $C_{54}H_{18}$ and $C_{96}H_{24}$ complexes with *n*-alkanes and *n*-perfluoroalkanes were optimised at the B3LYP/6-31G* level[46] with Grimme's D3 dispersion correction[47] (B3LYP-D3/6-31G*). First, the geometries of isolated $C_{54}H_{18}$ and $C_{96}H_{24}$ were optimised. The optimised geometries of $C_{54}H_{18}$ and $C_{96}H_{24}$ with all-trans *n*-alkanes and *n*-perfluoroalkanes were used to prepare the initial geometries of the $C_{54}H_{18}$ and $C_{96}H_{24}$ complexes with *n*-alkanes and *n*-perfluoroalkanes. The flat-on orientations were used for the initial geometries. The geometry of $C_{54}H_{18}$ and $C_{96}H_{24}$ was fixed during geometry optimisations of the complexes.

The intermolecular interaction energies (E_{int}) of $C_{54}H_{18}$ complexes with propane and perfluoropropane were calculated using dispersion-corrected DFT (B3LYP and some double hybrid functionals) and MP2 methods with different basis functions. The E_{int} was obtained with horizontally moving planar propane and perfluoropropane along the *x*- or *y*-axis from their positions in optimised structures of the complexes. The E_{int} of $C_{96}H_{24}$ complexes with *n*-alkanes and *n*-perfluoroalkanes were calculated by B3LYP-D3 in the same manner. The distances between the adsorbed molecules and π-plane of $C_{54}H_{18}$ or $C_{96}H_{24}$ were taken from the optimised geometries of the complexes (see Figs. 2 and S6), and the distances were fixed during calculations with the horizontal displacement. The basis set superposition error (BSSE)[48] was corrected in the calculations of the complexes using the counterpoise method.[49]

The change in the interaction energy (ΔE_{int}) was calculated as follows:

$$\Delta E_{int} = E_{int} - E_{int}(0),$$

where $E_{int}(0)$ represents the E_{int} calculated at the position in the optimised (stable) structure.

Results and discussion

Accuracy of B3LYP-D3 calculations.

The intermolecular interaction energies calculated at the CCSD(T) level using sufficiently large basis sets agree well with the gas-phase experimental values.[50] However, the CCSD(T) calculations are computationally too intensive to calculate the $C_{96}H_{24}$ complexes. Therefore, we evaluated the interaction energies of the $C_{96}H_{24}$ complexes using the B3LYP-D3 calculations in this study.

Although dispersion corrected DFT calculations do not require large computational resources, the calculated intermolecular interaction energies depend on the choice of functional and dispersion correction method.[51] Therefore, the choice of functional and dispersion correction method is significantly important. It has been reported that the B3LYP-D3 show sufficiently good performance in the calculations of the intermolecular interaction energies of aromatic molecules with alkanes and a perfluoroalkane.[30] The calculated interaction energies at the B3LYP-D3/6-311G** level are close to the estimated CCSD(T) level interaction energies at the basis set limit. Therefore, we used the B3LYP-D3 in this study.

In addition, we compared the ΔE_{int} calculated for $C_{54}H_{18}$ complexes with propane and perfluoropropane by the B3LYP-D3 with those obtained by the MP2 and dispersion-corrected double hybrid DFT calculations.[51] The ΔE_{int} obtained by the B3LYP-D3 calculations are close to those obtained by the MP2 and dispersion-corrected double hybrid DFT calculations (ESI). The details of the comparison are discussed later.

The ΔE_{int} values of propane and perfluoropropane associated with the horizontal displacement along *x*- and *y*-axis from the optimal position on the $C_{54}H_{18}$ were calculated by the B3LYP-D3 and MP2 methods using the 6-31G* and 6-311G** basis sets to evaluate the basis set dependence and the difference between the B3LYP-D3 and MP2 calculations. The medium size basis sets were selected for MP2 calculations, since the error cancellation of the overestimation of the dispersion interactions by the MP2 calculations compared with CCSD(T) calculations and the underestimation by the use of medium size basis sets compared with the complete basis set limit is expected.[53,54] The calculated E_{int} and ΔE_{int} are summarized in Tables S1–S4 and S5–S8, respectively. The plots of ΔE_{int} associated with the displacement along *x*-axis (Tables S5 and S6) are shown in Fig. 1, and those along *y*-axis (Tables S7 and S8) are shown in Fig. S1. The E_{int} values for the propane and perfluoropropane complexes obtained by the MP2 calculations show basis set dependence. The E_{int} values calculated at the

MP2/6-31G* level are less negative than those calculated at the MP2/6-311G* level, owing to the underestimation of the dispersion interactions using the small 6-31G* basis set. On the other hand, the basis set dependence of the E_{int} values obtained by the B3LYP-D3 calculations is almost negligible. The E_{int} values obtained by the B3LYP-D3 calculations are slightly more negative than those obtained by the MP2 calculations. The same tendency was reported in our previous work.[30] On the other hand, the basis set dependence of the ΔE_{int} is negligible and the ΔE_{int} values obtained by the B3LYP-D3 calculations are close to those obtained by the MP2 calculations, as shown in Figs. 1 and S1. Although the double hybrid DFT calculations are computationally more intensive than B3LYP calculations, the good performance of double hybrid DFT for calculating intermolecular interaction energies was suggested.[52] Therefore, we calculated the E_{int} and ΔE_{int} using dispersion corrected double hybrid DFT (B2PLYP and mPW2PLYP). The ΔE_{int} values obtained by B3LYP-D3 and MP2 calculations are close to those obtained by the dispersion-corrected double hybrid DFT calculations (Figs. S2 and S3). In addition, the ΔE_{int} values

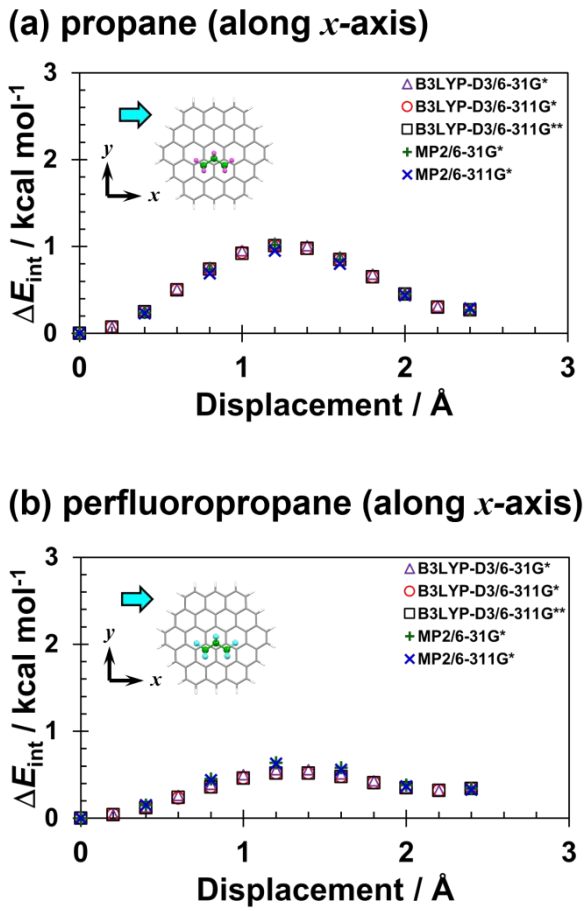

Fig. 1 Plots of ΔE_{int} for flat-on (a) propane and (b) perfluoropropane associated with horizontal displacements along *x*-axis obtained by dispersion-corrected DFT and MP2 calculations: purple triangles, red circles and black squares correspond to ΔE_{int} obtained by B3LYP-D3/6-31G*, B3LYP-D3/6-311G*, and B3LYP-D3/6-311G** level calculations, respectively; green plus and blue cross marks correspond to ΔE_{int} obtained by MP2/6-31G*, MP2/6-311G* level calculations, respectively.

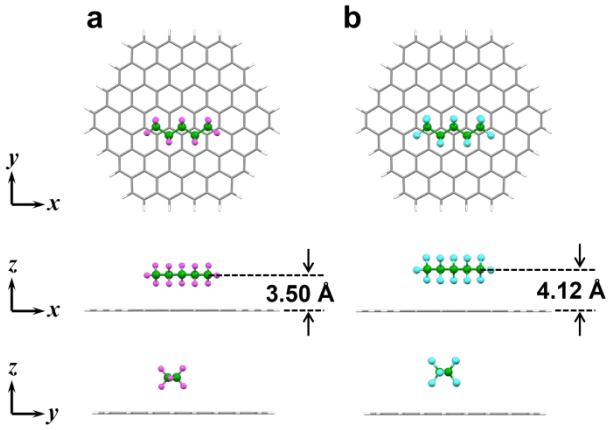

Fig. 2 Optimised geometries of $C_{96}H_{24}$ complexes with *n*-pentane and *n*-perfluoropentane, as viewed from three directions. The carbon, hydrogen, and fluorine atoms of adsorbed molecules are coloured in green, pink, and cyan, respectively.

calculated using B3LYP-D3 are close to those calculated using PBE0[55] and BLYP[56,57] functionals with D3 dispersion corrections (Tables S17, S18 and Fig. S4). Thus, the choice of calculation method has little effect on the calculated ΔE_{int}, and this fact suggests that the ΔE_{int} obtained by the B3LYP-D3 calculations are sufficiently accurate to discuss the alkyl chain length dependence of ΔE_{int} and the effect of fluorination on ΔE_{int}.

Geometry optimisation of $C_{96}H_{24}$ complexes with *n*-alkanes and *n*-perfluoroalkanes.

The geometries of $C_{96}H_{24}$ complexes with *n*-pentane and *n*-perfluoropentane were optimised. To confirm the stable positions of alkanes and perfluoroalkanes on the model graphite surface, energy calculations of $C_{54}H_{18}$ complexes with propane and perfluoropropane were carried out by scanning two-dimensionally (Fig. S5). The mean plane of the carbon atoms of *n*-pentane is parallel to the surface of $C_{96}H_{24}$ in the optimised geometry, as shown in Fig. 2(a). The hydrogen atoms of *n*-pentane are located near the centres of the six-membered rings of $C_{96}H_{24}$. This geometry is favourable for decreasing the distance between *n*-pentane and the π-plane of $C_{96}H_{24}$ and increasing the stabilization by the dispersion interactions.[30] The average distance of the carbon atoms of *n*-pentane from the π-plane of $C_{96}H_{24}$ in the optimised geometry is 3.50 Å. The fluorine atoms of *n*-perfluoropentane are also located near the centres of the six-membered rings of $C_{96}H_{24}$ in the optimised geometry (Fig. 2(b)), while the average distance of the carbon atoms of *n*-perfluoropentane from the π-plane of $C_{96}H_{24}$ is 4.12 Å, which is significantly larger than that of *n*-pentane. Apparently, larger atomic radius of fluorine compared with hydrogen is the primary cause of the larger intermolecular distance of *n*-perfluoropentane.[30] The calculated average distances of *n*-pentane and *n*-perfluoropentane in the $C_{96}H_{24}$ complexes are close to those calculated in the $C_{54}H_{18}$ complexes of *n*-pentane and *n*-perfluoropentane.[30] The optimised geometries of the

$C_{96}H_{24}$ complexes with propane, *n*-heptane, perfluoropropane and *n*-perfluoroheptane are shown in Fig. S6.

Change in interaction energy of *n*-pentane adsorbed on $C_{96}H_{24}$ associated with horizontal displacement.

The E_{int} was calculated at the B3LYP-D3/6-311G** level with changing the position of *n*-pentane on $C_{96}H_{24}$ horizontally along the *x*-axis from the position in the stable structure in steps of 0.2 Å (Figs. 3(a–c)), while keeping the distance from the π-plane of $C_{96}H_{24}$ (3.50 Å). The calculated E_{int} values are shown in Table S23. The ΔE_{int} values of *n*-pentane (Table S24) are plotted in Fig. 3(h) (cyan circles). The ΔE_{int} increases as *x* (displacement along *x*-axis) increases from 0.0 (a) to 1.2 Å (b), indicating that the adsorbed molecule becomes unstable. The ΔE_{int} reaches a maximum value (1.63 kcal mol^{-1}) when *x* = 1.2 Å (b). The carbon and hydrogen atoms of *n*-pentane projected onto $C_{96}H_{24}$ overlap with C–C bonds of $C_{96}H_{24}$. Then, the ΔE_{int} decreases, as *x* increases from 1.2 Å (b) to 2.4 Å (c). The ΔE_{int} is close to zero when *x* = 2.4 Å (c).

The E_{int} was also calculated by changing the position of *n*-pentane horizontally along the *y*-axis (Figs. 3(a, d–g)). The plot of ΔE_{int} (Fig. 3(h) (blue square)) has two maxima (1.82 and 1.85 kcal mol^{-1}, respectively) when *y* = 1.4 (d) and 3.0 Å (f) (*y* is displacement along *y*-axis). The projection of the hydrogen atoms of *n*-pentane overlapped with the carbon atoms of $C_{96}H_{24}$ in (d) and (f), and with C–C bonds of $C_{96}H_{24}$ when *y* = 2.2 Å (e). The ΔE_{int} (1.60 kcal mol^{-1}) in (e) is slightly smaller than those in (d) and (f). The ΔE_{int} is close to zero when *y* = 4.2 Å (g). The positions of carbon and hydrogen atoms of *n*-pentane relative to six-membered rings of $C_{96}H_{24}$ when y = 4.2 Å (g) are similar to those when y = 0.0 Å (a). These results clearly indicate that E_{int} of *n*-pentane changes significantly associated with horizontal displacement. The maximum value of ΔE_{int} ($\Delta E_{int(max)}$) when *x* = 1.2 Å (b) and those when *y* = 1.4 (d) and 3.0 Å (f) are close.

Change in interaction energy of *n*-perfluoropentane adsorbed on $C_{96}H_{24}$ associated with horizontal displacement.

The E_{int} was calculated at the B3LYP-D3/6-311G** level with Grimme's D3 dispersion correction with changing the position of *n*-perfluoropentane on $C_{96}H_{24}$ horizontally (Figs. 4(a–g)). The calculated E_{int} and ΔE_{int} values are summarized in Tables S23and S24, respectively. The shapes of the ΔE_{int} plots are similar to those of *n*-pentane. The plot associated with the displacement along the *y*-axis (Figs. 4(d–h)) has a maximum (0.68 kcal mol^{-1}) when *x* = 1.2 Å (b) as shown in Fig. 4h as in the case of *n*-pentane. The shape of the plot of ΔE_{int} associated with the displacement along the *y*-axis (Figs. 4(d–h)) is similar to that of *n*-pentane. The plot has maxima when *y* = 1.4 (d) and 3.0 Å (f) as in the case of *n*-pentane. The ΔE_{int} at (d) and (f) are 0.83 and 0.92 kcal mol^{-1}, respectively. The maximum ΔE_{int} associated

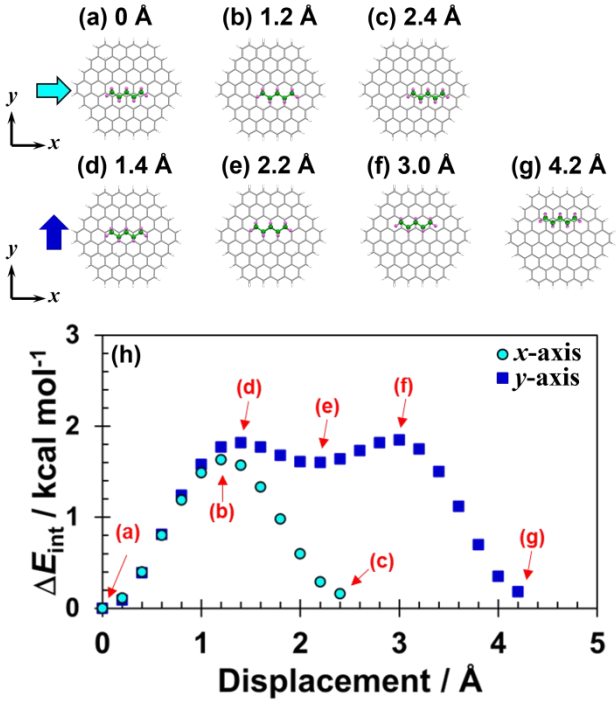

Fig. 3 Geometries of $C_{96}H_{24}$ complexes with *n*-pentane and plots of ΔE_{int}: (a) Geometry of complex at the optimal position; (b, c) *n*-pentane was moved horizontally 1.2 and 2.4 Å along *x*-axis, respectively ; (d–g) *n*-pentane was moved horizontally 1.4, 2.2, 3.0, and 4.2 Å along *y*-axis, respectively; (h) Plots of ΔE_{int} for *n*-pentane associated with horizontal displacement obtained by B3LYP-D3/6-311G** level calculations. The cyan circles and blue squares correspond to ΔE_{int} associated with displacement along *x*- and *y*-axes, respectively.

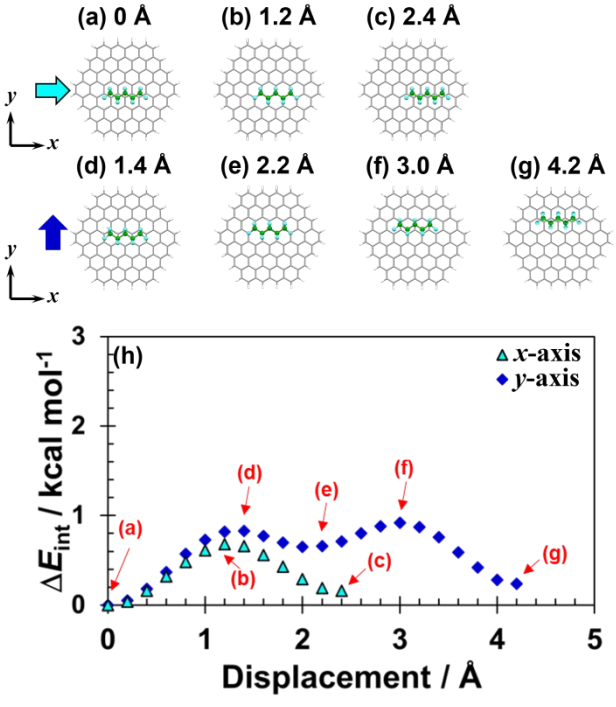

Fig. 4 Geometries of $C_{96}H_{24}$ complexes with *n*-perfluoropentane and plots of ΔE_{int}: (a) Geometry of complex at the optimal position ; (b, c) *n*-perfluoropentane was moved horizontally 1.2 and 2.4 Å along *x*-axis, respectively; (d–g) *n*-perfluoropentane was moved horizontally 1.4, 2.2, 3.0, and 4.2 Å along *y*-axis, respectively; (h) Plots ΔE_{int} for *n*-perfluoropentane associated with horizontal displacement obtained by B3LYP-D3/6-311G** level calculations. The cyan triangles and blue rhombi correspond to ΔE_{int} associated with displacement along *x*- and *y*-axes, respectively.

with the displacement along the *x*-axis at (b) (0.68 kcal mol^{-1}) is approximately 42% that of *n*-pentane. The maximum ΔE_{int} values associated with the displacement along the *y*-axis at (d) and (f) calculated for *n*-perfluoropentane were 46% and 50% of those calculated for *n*-pentane, respectively. These results clearly show that the changes in E_{int} for *n*-perfluoropentane associated with horizontal displacement are significantly smaller than those for *n*-pentane. The E_{int} for *n*-pentane and *n*-perfluoropentane at (a) are –11.63 and –9.30 kcal mol^{-1}, respectively. The E_{int} for *n*-perfluoropentane is 80 % of that for *n*-pentane. The impact of fluorination on ΔE_{int} (50–58 % decrease) is stronger than that on E_{int} (20 % decrease).

Origin of ΔE_{int} change associated with horizontal displacement.

The E_{int} can be decomposed into each energy term such as electrostatic (E_{es}), induction (E_{ind}), short-range (E_{short}, mainly exchange-repulsion) and dispersion (E_{disp}) interactions. To elucidate the cause of the change in ΔE_{int} with horizontal displacement shown in Figs. 3 and 4, the contributions of the change in each energy term for *n*-pentane and *n*-perfluoropentane on $C_{96}H_{24}$, were analysed while moving horizontally along *x*- and *y*-axes. Details of the energy decomposition procedure are shown in ESI. The calculated values of each energy term are listed in Tables S25 and S26. Fig. S7 shows the plots of each energy term as a function of horizontal displacement along *x*- and *y*-axes. The E_{es} and E_{ind} are small and nearly constant during the displacement. The E_{disp} is the main contributor of the attraction and are almost constant. In contrast, the E_{short} shows large changes associated with the displacement. The shapes of the plots of E_{int} and E_{short} are synchronized as shown in Fig. S7, suggesting that change in the ΔE_{int} (= E_{int} – $E_{int}(0)$) values associated with the horizontal displacement in Figs. 3 and 4 is mainly determined by the change in the E_{short}. The difference between maximum and minimum values of E_{short} (ΔE_{short}) for *n*-pentane is larger than that of *n*-perfluoropentane. The ΔE_{short} for *n*-pentane along *y*-axis is 2.30 kcal mol^{-1}, whereas that for *n*-perfluoropentane is 0.76 kcal mol^{-1}, as shown in Table S26. This difference suggests that *n*-alkanes have stronger resistance against horizontal displacement compared with corresponding *n*-perfluoroalkanes owing to the larger change of E_{short} associated with the displacement.

Effect of alkyl chain length.

The geometries of $C_{96}H_{24}$ complexes with propane, *n*-heptane, perfluoropropane, and *n*-perfluoroheptane were optimised. The average distances between the carbon atoms of the four molecules and the π-plane of $C_{96}H_{24}$ are shown in Fig. S6. The E_{int} and ΔE_{int} were calculated at the B3LYP-D3/6-311G** level with horizontally changing the positions of the planar four molecules on $C_{96}H_{24}$ as shown in Tables S23 and S24, respectively. The distances between the adsorbed molecules and the π-plane of $C_{96}H_{24}$ were fixed in the calculations. The shapes of the plots of ΔE_{int} for the four molecules are similar to those for *n*-pentane and *n*-perfluoropentane, as shown in Fig. 5. The plots obtained associated with the displacement along the *x*-axis have a maximum when *x* = 1.2 Å, while those obtained

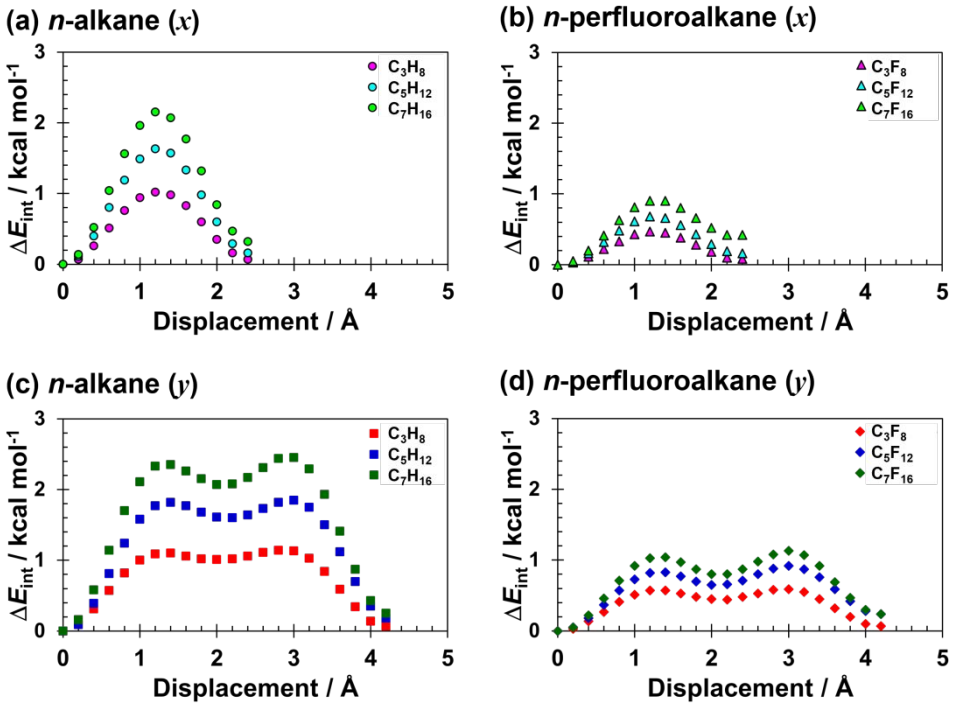

Fig. 5 Changes in ΔE_{int} of *n*-alkanes (a, c) and *n*-perfluoroalkanes (b, d) associated with horizontal displacement obtained by B3LYP-D3/6-311G** level calculations: (a) Changes in ΔE_{int} for propane, *n*-pentane and *n*-heptane (pink, cyan and light green circles) by displacements along *x*-axis; (b) Changes in ΔE_{int} for perfluoropropane, *n*-perfluoropentane and *n*-perfluoroheptane (pink, cyan and light green triangles) by displacements along *x*-axis; (c) Changes in ΔE_{int} for three alkanes (red, blue and green squares) by displacements along *y*-axis; (d) Changes in ΔE_{int} for three perfluoroalkanes (red, blue and green rhombi) by displacements along *y*-axis.

associated with the displacement along the *y*-axis have two maxima when *y* = 1.4 and 3.0 Å. The ΔE_{int} when *x* = 1.2 Å and *y* = 1.4 Å ($\Delta E_{int(max)}$) are highlighted in Table S10. The longer the chain length, the larger the $\Delta E_{int(max)}$ value. The chain length dependence of $\Delta E_{int(max)}$ of *n*-alkanes is stronger than that of *n*-perfluoroalkanes, as shown in Fig. 5. The $\Delta E_{int(max)}$ values for propane, *n*-pentane, and *n*-heptane at *y* = 1.4 Å are 1.10, 1.82, and 2.35 kcal mol^{-1}, respectively. The $\Delta E_{int(max)}$ values for *n*-pentane and *n*-heptane are 65% and 114% larger than that for propane. The $\Delta E_{int(max)}$ values for perfluoropropane, *n*-perfluoropentane, and *n*-perfluoroheptane at *y* = 1.4 Å are 0.57, 0.83, and 1.04 kcal mol^{-1}, respectively. The $\Delta E_{int(max)}$ values for *n*-perfluoropentane and *n*-perfluoroheptane were 46% and 82% larger than that for perfluoropropane.

The different chain length dependence of the $\Delta E_{int(max)}$ values for *n*-alkanes and *n*-perfluorlalkanes is further evident by plotting the $\Delta E_{int(max)}$ when *x* = 1.2 Å and *y* = 1.4 Å, as shown in Fig. 6. The $\Delta E_{int(max)}$ values when *y* = 1.4 Å (displacement along the *y*-axis) are always slightly larger than those when *x* = 1.2 Å (displacement along the *x*-axis), regardless of the chain length. The $\Delta E_{int(max)}$ value per carbon atom of the *n*-alkanes (ca. 0.30 kcal mol^{-1}) is approximately 2.5 times as large as that of *n*-perfluoroalkanes (ca. 0.12 kcal mol^{-1}).

Although $\Delta E_{int(max)}$ associated with the horizontal displacement is not exactly the barrier height for the horizontal motion, we can expect that the $\Delta E_{int(max)}$ values correlate with the barrier heights. In the former section, it was found that the ΔE_{int} change in accordance with the E_{short}, suggesting that the barrier is mainly determined by the short-range interactions. The calculated $\Delta E_{int(max)}$ values suggest that the barrier heights associated with the horizontal motion of adsorbed *n*-alkanes and *n*-perfluorlalkanes on graphite increased as the chain length increased, and that the barrier heights of the horizontal motion of *n*-alkanes are higher than those of the corresponding *n*-perfluoroalkanes probably due to the larger changes of short-range interactions. Therefore, *n*-perfluoroalkanes move and slide more readily than *n*-alkanes on graphite materials, resulting in the formation of less-stable interfacial structures.

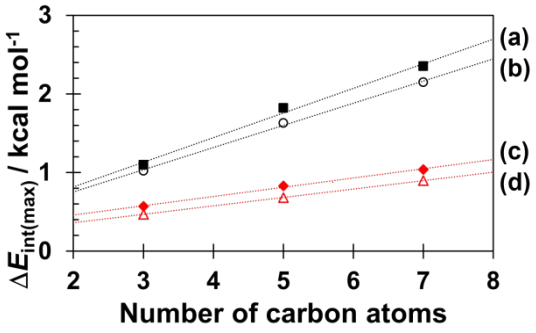

Fig. 6 Chain length dependence of $\Delta E_{int(max)}$ (maximum ΔE_{int} associated with horizontal displacement) obtained by B3LYP-D3/6-311G** level calculations: (a) $\Delta E_{int(max)}$ for *n*-alkanes associated with displacement along *y*-axis (black square) $\Delta E_{int(max)} = 0.31N + 0.19$ (*N* is number of carbon atoms); (b) $\Delta E_{int(max)}$ for *n*-alkanes associated with displacement along *x*-axis (black circle), $\Delta E_{int(max)} = 0.28N + 0.19$; (c) $\Delta E_{int(max)}$ for *n*-perfluoroalkanes associated with displacement along *y*-axis (red rhombi), $\Delta E_{int(max)} = 0.12N + 0.23$; (d) $\Delta E_{int(max)}$) for *n*-perfluoroalkanes associated with displacement along *x*-axis (red triangle), $\Delta E_{int(max)} = 0.11N + 0.15$ (kcal mol^{-1}).

Conclusions

The dispersion-corrected DFT and MP2 calculations were applied to evaluate the intermolecular interaction energies (E_{int}) of *n*-alkanes and *n*-perfluoroalkanes with $C_{54}H_{18}$ and $C_{96}H_{24}$ as a model of adsorption on the graphite surface. The changes in E_{int} associated with the horizontal displacement of *n*-alkanes and *n*-perfluoroalkanes on the $C_{54}H_{18}$ and $C_{96}H_{24}$ surface (ΔE_{int}) were evaluated. The ΔE_{int} values associated with the horizontal displacements obtained by the B3LYP-D3 calculations are close to those obtained by the MP2 and dispersion-corrected double hybrid DFT calculations. The dispersion interactions are responsible for the attraction between adsorbed molecule and graphite model surface, whereas the change in ΔE_{int} values associated with horizontal displacement is mainly determined by the short-range interactions. The maximum values of ΔE_{int} ($\Delta E_{int(max)}$) increases as the chain length increases. The $\Delta E_{int(max)}$ values for the *n*-alkanes are significantly larger than those for the corresponding *n*-perfluoroalkanes owing to the different magnitude of short-range interactions. These results suggest that the barrier heights of the horizontal motion of *n*-alkanes on the graphite surface are higher than those of the corresponding *n*-perfluoroalkanes and the barrier height increases as the chain length increases.

The present results on the changes in ΔE_{int} with horizontal displacements of *n*-alkanes and *n*-perfluoroalkanes are essential information for understanding the stability of adsorbed species containing alkyl or fluoroalkyl chains against horizontal movement. Furthermore, this fundamental information is expected to contribute to the development of new materials for surface self-assemblies and coatings.

Author Contributions

Yoshihiro Kikkawa: Conceptualization, Methodology, Data curation, Formal analysis, Investigation, Visualization, Writing – original draft, Writing – review & editing. Seiji Tsuzuki: Conceptualization, Methodology, Data curation, Formal analysis, Investigation, Visualization, Writing – original draft, Writing – review & editing.

Conflicts of interest

There are no conflicts to declare.

Acknowledgements

This work was partially supported by JSPS KAKENHI (JP23H01702 to Y. K.) and JST CREST (JPMJCR18J2 to S.T.).

Notes and references

1 R. K. Smith, P. A. Lewis and P. S. Weiss, *Prog. Surf. Sci.*, 2004 **75**, 1–68 (2004).

2 M. Kind and C. Wöll, *Prog. Surf. Sci.,* 2009, **84**, 230–278.
3 D. B. Amabilino, *Supramolecular Chemistry at Surfaces*, Royal Society of Chemistry, London, 2016
4 Y. Meng, J. Xu, L. Ma, Z. Jin, B. Prakash, T. Ma and W. Wang, *Friction*, 2022, **10**, 1443–1595.
5 L. E. Bailey, K. K. Kanazawa, G. Bhatara, G. W. Tyndall, M. Kreiter, W. Knoll and C. W. Frank, Langmuir, 2001, **17**, 8145–8155.
6 K. Miyake, Y. Hori, T. Ikeda, M. Asakawa, T. Shimizu, T. Ishida and S. Sasaki, *Jpn. J. Appl. Phys*., 2005, 44, 5403–5408.
7 M.-D. Krass, G. Krämer, U. Dellwo and R. Bennewitz, *Tribol. Lett.*, 2018, **66**, 87.
8 A. A. Vasko, V. Y. Kutsenko, A. A. Marchenko and O. M. Braun, *Tribol. Lett*., 2019, **67**, 49.
9 J. Li, W. Cao, J. Li, M. Ma and J. Luo, *J. Phys. Chem. Lett.*, 2019, **10**, 2978–2984.
10 M. Giese and M. Albrecht, *ChemPlusChem*, 2020, **85**, 715–724.
11 T. Taira, *J. Oleo Sci.*, 2022, **71**, 167–175.
12 N. Davison and E. Lu, *Dalton Trans.*, 2023, **52**, 8172–8192.
13 S. Liu, Y. Norikane and Y. Kikkawa, *Beilstein J. Nanotechnol.,* 2023, **14**, 872–892.
14 J. Pu, S. Wan, W. Zhao, Y. Mo, X. Zhang, L. Wang and Q. Xue, *J. Phys. Chem. C*, 2011, **115**, 13275–13284.
15 T. Carstens, R. Gustus, O. Höfft, N. Borisenko, F. Endres, H. Li, R. J. Wood, A. J. Page and R. Atkin, *J. Phys. Chem. C*, 2014, **118**, 10833–10843.
16 K. Iritani, K. Tahara, S. De Feyter and Y. Tobe, *Langmuir*, 2017 **33**, 4601–4618.
17 P. Karipoth, A. Pullanchiyodan, A. Christou and R. Dahiya, *ACS Appl. Mater. Interfaces*, 2021, **13**, 61610–61619.
18 L. Verstraete and S. De Feyter, *Chem. Soc. Rev.*, 2021, **50**, 5884–5897.
19 K. R. Paserba and A. J. Gellman, *Phys. Rev. Lett.*, 2001, **86**, 4338–4341.
20 K. R. Paserba and A. J. Gellman, *J. Chem. Phys.*, 2001, **115**, 6737–6751.
21 A. J. Gellman and K. R. Paserba, *J. Phys. Chem. B*, 2002, **106**, 13231–13241.
22 R. Zacharia, H. Ulbricht and T. Hertel, *Phys. Rev.* B, 2004, **69**, 155406.
23 H. Ulbricht, R. Zacharia, N. Cindir and T. Hertel, *Carbon*, 2006, **44**, 2931–2942.
24 S. L. Tait, Z. Dohnálek, C. T. Campbell and B. D. Kay, *J. Chem. Phys*., 2006, 125, 234308.
25 C. Thierfelder, M. Witte, S. Blankenburg, E. Rauls and W. G. Schmidt, *Surf. Sci*., 2011, **605**, 746–749.
26 E. Londero, E. K. Karlson, M. Landahl, D. Ostrovskii, J. D. Rydberg and E. Schröder, *J. Phys. Condens. Matter*, 2012, **24**, 424212.
27 K. Kamiya and S. Okada, *Jpn. J. Appl. Phys.*, 2013, **52** 04CN07.
28 S. Conti and M. Cecchini, *J. Phys. Chem. C*, 2015, **119**, 1867–1879.
29 L. Verstraete, T. Rinkovec, H. Cao, H. I. Reeves, J. N. Harvey and S. De Feyter, *J. Phys. Chem. C*, 2021, **125**, 1557–1563.
30 Y. Kikkawa and S. Tsuzuki, *Phys. Chem. Chem. Phys*., 2023, **25**, 11331–11337.
31 J. A. A. W. Elemans, *Adv. Funct. Mater*., 2016, **26**, 8932–8951.
32 J. Teyssandier, K. S. Mali and S. De Feyter, *ChemistryOpen*, 2020, 9, 225–241.
33 Y. Tobe, K. Tahara and S. De Feyter, *Chem. Commun.*, 2021, **57**, 962–977.
34 L. Verstraete and S. De Feyter, *Chem. Soc. Rev.*, 2021, **50**, 5884–5897.
35 B. Ilan, G. M. Florio, M. S. Hybertsen, B. J. Berne and G. W. Flynn, *Nano Lett.*, 2008, **8**, 3160–3165.
36 T. Yang, S. Berber, J. F. Liu, G. P. Miller and D. Tománek, *J. Chem. Phys*., 2008, **128**, 124709.
37 A. Stabel, L. Dasaradhi, D. O'Hagan and J. P. Rabe, *Langmuir*, 1995, **11**, 1427–1430.
38 C. L. Claypool, F. Faglioni, W. A. Goddard, H. B. Gray, N. S. Lewis and R. A. Marcus, *J. Phys. Chem. B,* 1997, **101**, 5978–5995.
39 R. Lazzaroni, A. Calderone, J. L. Brédas and J. P. Rabe, *J. Chem. Phys.*, 1997, **107**, 99–105.
40 A. Gesquière, M. M. Abdel-Mottaleb, F. C. De Schryver, M. Sieffert and K. Müllen, *Langmuir*, 1999, **15**, 6821–6824.
41 M. M. S. Abdel-Mottaleb, S. De Feyter, M. Sieffert, M. Klapper, K. Müllen and F. C. De Schryver, *Langmuir*, 2003, **19**, 8256–8261.
42 A. Gesquière, M. M. Abdel-Mottaleb, S. De Feyter, F. C. De Schryver, M. Sieffert, K. Müllen, A. Calderone, R. Lazzaroni and J.-L. Brédas, *Chem. Eur. J.*, 2000, **6**, 3739–3746.
43 Y. Kikkawa, S. Tsuzuki, K. Taguchi, A. Kashiwada and K. Hiratani, *Phys. Chem. Chem. Phys*., 2017, **19**, 13579–13584.
44 J. E. Parker, S. M. Clarke and A. C. Perdigón, *Surf. Sci.*, 2007, **601**, 4149–4153.
45 M. J. Frisch, G. W. Trucks, H. B. Schlegel, G. E. Scuseria, M. A. Robb, J. R. Cheeseman, G. Scalmani, V. Barone, G. A. Petersson, H. Nakatsuji, X. Li, M. Caricato, A. V. Marenich, J. Bloino, B. G. Janesko, R. Gomperts, B. Mennucci, H. P. Hratchian, J. V. Ortiz, A. F. Izmaylov, J. L. Sonnenberg, D. Williams-Young, F. Ding, F. Lipparini, F. Egidi, J. Goings, B. Peng, A. Petrone, T. Henderson, D. Ranasinghe, V. G. Zakrzewski, J. Gao, N. Rega, G. Zheng, W. Liang, M. Hada, M. Ehara, K. Toyota, R. Fukuda, J. Hasegawa, M. Ishida, T. Nakajima, Y. Honda, O. Kitao, H. Nakai, T. Vreven, K. Throssell, J. A. Montgomery, Jr., J. E. Peralta, F. Ogliaro, M. J. Bearpark, J. J. Heyd, E. N. Brothers, K. N. Kudin, V. N. Staroverov, T. A. Keith, R. Kobayashi, J. Normand, K. Raghavachari, A. P. Rendell, J. C. Burant, S. S. Iyengar, J. Tomasi, M. Cossi, J. M. Millam, M. Klene, C. Adamo, R. Cammi, J. W. Ochterski, R. L. Martin, K. Morokuma, O. Farkas, J. B. Foresman and D. J. Fox, *Gaussian16*, *Revision C. 01*, Gaussian, Inc., Wallingford, CT, 2016.
46 A. D. Becke, *J. Chem. Phys.*, 1993, **98**, 5648–5652.
47 S. Grimme, J. Antony, S. Ehrlich and H. Krieg, *J. Chem. Phys*., 2010, **132**, 154104.
48 B. J. Ransil, *J. Chem. Phys.*, 1961, **34**, 2109–2118.
49 S. F. Boys and F. Bernardi, *Mol. Phys.*,1970, **19**, 553–566.
50 T. H. Dunning, Jr., *J. Phys. Chem. A*, 2000, **104**, 9062–9080.
51 S. Tsuzuki, T. Uchimaru, *Phys. Chem. Chem. Phys.*, 2020, **22**, 22508-22519.
52 L. Goerigk and Stefan Grimme, *J. Chem. Theory Comput.,* 2011, **7**, 291–309.
53 S. Tsuzuki, K. Honda, T. Uchimaru, M. Mikami and K. Tanabe, *J. Am. Chem. Soc.*, 2002, **124**, 104.
54 K. Shibasaki, A. Fujii, N. Mikami and S. Tsuzuki, *J. Phys. Chem. A*, 2006, **110**, 4397.
55 C. Adamo and V. Barone, *J. Chem. Phys*., 1999, **110**, 6158–6169.
56 A. D. Becke, *Phys. Rev. A: At., Mol., Opt. Phys.*, 1988, **38**, 3098–3100.
57 C. Lee, W. Yang and R. G. Parr, *Phys. Rev. B: Condens. Matter Mater. Phys.*, 1988, **37**, 785–789.

The data supporting this article have been included as part of the Supplementary Information.